applied sciences

MDPI

Article

Research on the Impact Force of Rockfall Impacting Sand Cushions with Different Shapes

Yu Zhang [1], Lingzhi Xie [1,2,*], Bo He [2] and Peng Zhao [1]

[1] State Key Laboratory of Hydraulic and Mountain River Engineering, College of Architecture and Environment, Sichuan University, Chengdu 610065, China; zhangyu3@stu.scu.edu.cn (Y.Z.); scu_zhaopeng@163.com (P.Z.)

[2] Institute of New Energy and Low-Carbon Technology, Sichuan University, Chengdu 610065, China; hebo@scu.edu.cn

* Correspondence: xielingzhi@scu.edu.cn; Tel.: +86-130-7602-3636

Abstract: Shed structures are an important engineering method for mountain highways to resist rockfall impacts. Research on the rockfall impact response is very important to the design of rockfall disaster protection structures to shed cave structures. To explore the impact difference caused by different rockfall shapes, five mortar ellipsoids were fabricated with different shapes by 3D printing the falling stone mould. Laboratory experiments were carried out to study the impact effect of five different shapes of falling stones on the sand cushion. Different shapes of rockfall correspond to different impact forces. The tip ellipsoid (D1 and D2) is the smallest, the sphere (D3) is the second, and the flat ellipsoid (D4 and D5) is the largest. The fitting analysis of the impact force results of the laboratory experiment showed that the impact of the falling height on the impact force was relatively independent and did not change with the shape of the falling rock. Then, based on the impact force of the sphere falling rock, a calculation formula of the impact force with the introduction of the shape factor was obtained, and it was compared and verified with the test results from other studies. To study the applicability of the formula in the actual engineering scale, a numerical model was established by ANSYS. After verifying the reliability of the numerical model, the impact process of a large energy level was simulated. According to the simulation results, the rationality of the formula proposed in this paper is further verified, which guides the actual rockfall impact prevention and control engineering.

Keywords: rockfall impact; rockfall shape; impact force; falling height; numerical simulation

Citation: Zhang, Y.; Xie, L.; He, B.; Zhao, P. Research on the Impact Force of Rockfall Impacting Sand Cushions with Different Shapes. *Appl. Sci.* **2022**, *12*, 3540. https://doi.org/10.3390/app12073540

Academic Editor: Laurent Daudeville

Received: 17 February 2022
Accepted: 29 March 2022
Published: 30 March 2022

1. Introduction

The entrance section of a highway tunnel in mountainous areas is a frequent area of rockfall disasters. Rockfall disasters are characterized by high frequency, multiple types, large scale, wide distribution, serious harm, strong randomness, and unpredictability. In recent years, there have been many incidents caused by falling rocks. Rockfall disaster has become an important factor restricting the development of the national economy and threatening people's lives and property safety [1]. At present, the shed-tunnel structure has been widely used as a passive protection measure [2,3] The shed hole is mainly composed of beams and plates in the rigid frame, and the buffer layer is laid on the upper part of the plate. The sand cushion is often used in engineering to disperse and absorb impact energy [4]. To avoid structural damage caused by the rockfall's impact force exceeding the bearing capacity of the shed tunnel structure and to ensure the stability of the shed tunnel structure, the shed tunnel structure should be able to withstand certain impact loads. Many scholars have studied the dynamic response of rockfall impact by different means [5–8].

Rockfall quality, falling height, rockfall shape, incident angle, buffer layer performance, etc. all affect the impact force of rockfalls. Most existing studies on the impact force have simplified the rockfall as a sphere [9,10] and have mainly considered the impact of the rockfall mass and falling height on the rockfall impact force [11]. The impact force increases with the mass and falling height. [7]. However, rockfall shapes are diverse [12], ranging from spheres to ellipsoids, cubes, and cylinders. Di Luzio et al. [13] showed the falling rocks with different volumes and shapes on the volcanic rock slab of the ancient Apia route: wedge-shaped, sub-cubic, sub-cubic and prismatic, and parallelepiped-shaped. When different shape rockfalls are in contact with the cushion, they may be in contact with the cushion by a point, a line, or a surface [14]. Different contact areas produce different impact effects, resulting in different impact forces acting on the structure. However, at present, few studies have considered the influence of rockfall shape on impact force. Perera et al. [15] designed a rockfall impact test with random shapes. The results show that the rockfall impact force has strong randomness, but there is no conclusion on which shape of rockfall will cause greater impact. Chen et al. [16] combined the impulse theorem and the finite element method to simplify rockfalls into three typical shapes (sphere, cube, and regular icosahedron with chamfered corners) and deduced the method considering various factors, such as the shape of the rockfall. The impact force formula of a rockfall acting on a reinforced concrete shed shows that the shape of the rockfall has a great influence on the impact force and impact time. Yan et al. [17] and Shen et al. [18] simplified the rockfall as an ellipsoid and used a numerical method to explore the impact of rockfall shape on the impact effect. The results showed that the rockfall shape had a great influence on the impact dynamic response, including impact force and impact duration and depression depth. Ji et al. [19] specially designed a rockfall collision device to realistically simulate the rockfall impact process. The results of laboratory experiments showed that the shape of the rockfall had a significant effect on the coefficient of restitution, and a new quantitative index of rockfall shape was proposed, namely, the shape factor. Yan et al. [20] carried out an experimental study of three typical shapes of rockfall impact cushions, spherical, conical, and flat, and their results showed that the rockfall shape had a significant impact on the impact test results. Yu et al. [21] cited the concept of sphericity and used numerical methods to study the maximum elongation of the flexible guardrail, the peak impact force, the peak force of the uphill anchor cable, the peak force of the lower main support cable, and the pile. The axial peak force of the column and the peak shear force of the pile foundation had a significant effect, and the spherical or polyhedral block assumption in the test standard may cause the protection failure of the flexible rockfall. The above research discussed the rockfall shape on impact effect, showing the importance of considering the effect of rockfall shape on the impact force. However, most of them only discussed several typical shapes and failed to take all the common falling stone shapes into account.

Rockfall impact force is a very important factor in the design of the shed tunnel structure [22]. In the commonly used impact force calculation formulas, the influencing factor of shape was not introduced and has some certain limitations. Common impact force algorithms are shown in Table 1. According to the current research, the impact force results are mostly the average impact force of the impact process or obtained by fitting the test data. Moreover, the shape of rockfall is ignored when calculating the impact force of rockfall. Existing research shows that it is inaccurate and unsafe to restore the falling rock to a sphere. Therefore, it is urgent to accurately calculate the impact force of rockfall impact shed tunnel cushion.

In this paper, falling rock is simplified into three categories: tip ellipsoid, sphere, and flat ellipsoid. The influence of different falling rock shapes on the impact force of falling rock is explored by laboratory experiments. Through a fitting analysis of the experimental results, the law in which the influence of falling height on the impact force of falling rock does not change the shape of falling rock is obtained. The formula for calculating the impact force of falling rock considering the shape of falling rock is further fitted. The accuracy of the numerical model is corrected by comparison with laboratory experimental results. In this way, the impact process of a larger size rockfall is simulated; further, the reliability of the fitting formula is verified. The applicability of the fitting formula is promoted to guide the calculation of rockfall impact force in practical engineering.

Table 1. Comparison of common impact force algorithms.

Algorithms	Principles	Advantages	Disadvantages
Ministry of Transport of the People's Republic of China [23]	Work-energy principle	Widely used in roadbed protection in China	1. Not maximum impact force 2. Not considered cushion thickness
Yang et al. [24]	Newton's law and laboratory impact test	Comprehensive consideration of rockfall quality, cushion thickness and impact velocity	1. Not maximum impact force 2. Smaller scale of experiments
Labiouse et al. [11] Kawahara et al. [25]	On-site impulse test	1. Good reliability 2. Simple calculation 3. Basically reflect the impact factors of rockfall	1. Only considered frontal collision 2. Depend heavily on the empirical values of the relevant constants

2. Experimental Design

This paper mainly considers the impact force of falling rock on the cushion of the shed tunnel, without considering the effect on concrete slab and frame. The sand with relatively easy access and large porosity was selected as the cushion material. This laboratory experiment was completed on the impact experimental device independently developed by Sichuan University.

2.1. Experimental Device

The experimental device of the drop hammer impact sand cushion experiment is mainly divided into the impact system and the acquisition system, as shown in Figure 1.

The impact system is mainly divided into three parts, including the falling device, falling stone, and sand box. The falling device is connected to the falling rock by an electromagnet, and the falling rock is released by a power outage. The electromagnet is located directly above the centre of the sand box to ensure that the falling rock impacts the centre of the sand box. The falling height is controlled by an electric hoist and measured by a laser rangefinder. The maximum falling height of the device is approximately 1.5 m.

The acquisition system is mainly composed of an acceleration sensor and dynamic signal acquisition instrument. The acquisition instrument adopts the dynamic signal tester with the DH5922D model produced by Donghua Testing Technology Co., Ltd. (Jingjiang, China), and the acceleration sensor adopts the IEPE piezoelectric acceleration sensor with the 1A531E model produced by Donghua Testing Technology Co., Ltd., which is installed on the upper surface of the drop hammer. The change in the drop hammer acceleration with time is collected through the DHDAS dynamic signal acquisition and analysis system. According to Newton's second and third laws and ignoring the drop hammer gravity, the maximum impact force of the drop hammer is the product of the maximum acceleration of the drop hammer and the drop hammer mass.

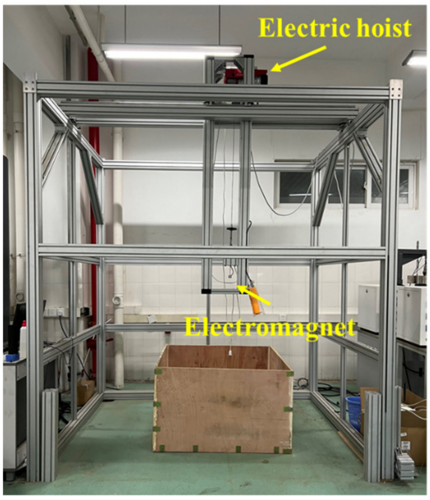

(**a**)

(**b**)

(**c**)

Figure 1. Experimental device. (**a**) Impact system, (**b**) dynamic signal acquisition instrument, and (**c**) IEPE piezoelectric acceleration sensor.

2.2. Experimental Program

To study the influence of different rockfall shapes on the impact effect of the shed cave cushion, five kinds of ellipsoid-shaped rockfalls were used to conduct experiments. Considering that the top of the rockfall needs to attract the electromagnet and the placement of the acceleration sensor, the ellipsoid in the upper half of the rockfall is replaced by a cylinder of equal mass. The height of the cylinder is h, and the diameter d of the cylinder is the maximum diameter of the falling rock in the vertical direction with the falling direction. The radius of the rockfall in the falling direction is b, and a coefficient $S = b/(d/2)$ is defined to describe the shape. The mould of resin material is obtained by 3D printing, and the falling stone is obtained by pouring mortar into the mould, curing, and demoulding, as shown in Figure 2.

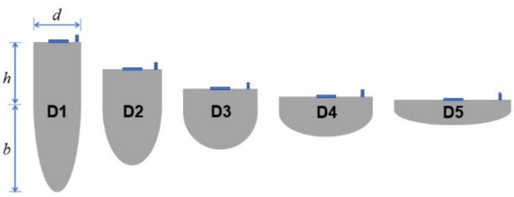

(**a**)

(**b**)

(**c**)

Figure 2. The production of falling stones used in laboratory experiments. (**a**) The schematic diagram of rockfall, (**b**) 3D printing mould, and (**c**) the rockfall obtained after pouring, curing, and demoulding.

The mass of falling rocks in the five shapes is approximately 1.65 kg. The specific values and the specific sizes of each shape are shown in Table 2, including two kinds of tip ellipsoids (D1 and D2), spheres (D3), and two kinds of flat ellipsoids (D4 and D5). During pouring, an M5 steel tooth rod is embedded on the rockfall surface to connect with the acceleration sensor. The rockfall is maintained for 28 days. After maintenance, the centre of the upper surface of the rockfall is polished to a level, and the iron sheet is affixed to absorb the electromagnet.

Table 2. Drop hammer mass and size.

No.	*m* (kg)	*h* (mm)	*d* (mm)	*b* (mm)	*S*
D1	1.629	96	72	144	4
D2	1.612	60	90	90	2
D3	1.696	38	114	57	1
D4	1.633	24	144	36	0.5
D5	1.677	15	180	22.5	0.25

The falling heights are 0.15 m, 0.3 m, 0.6 m, 0.9 m, and 1.2 m, respectively. The sandbox is surrounded by five 10 mm thick boards, and the inner size is 1 m $\times$ 1 m $\times$ 0.6 m. Seguin et al. [26] mentioned that when the sandbox size and falling stone diameter ratio are more than 5, the influence of the cushion lateral boundary constraint can be ignored. In this paper, the maximum diameter of falling stone is 0.18 m, and the ratio is 5.56 > 5; therefore, it can be considered that the sandbox is large enough, and the influence of the sandbox constraint can be ignored. There is a 6-mm thick steel plate at the bottom of the sand box, which can be regarded as a rigid constraint. To ensure that the rockfall impact is not affected by the bottom constraint of the cushion, the thickness of the sand cushion is selected as 0.3 m. Dry coarse yellow sand is used. The elastic modulus of sand is about 39 MPa. The sand cushion is naturally compacted by gravity.

The whole experimental process is as follows. First, the acceleration sensor is installed on the embedded steel tooth bar on the top of the falling rock, and the acceleration sensor is connected to the acquisition instrument. The falling rock is absorbed by the electromagnet in the falling device. The distance from the lowest point of the falling rock to the surface of the cushion is measured, namely, the falling height. At this time, the signal is collected, and the falling rock is released by breaking the power of the electromagnet. After the falling rock contacts the cushion, the acquisition signal is stopped, and the data are saved to complete a shock of the falling rock. Before the next impact, to prevent the material strength and density of the sand cushion from changing due to impact compaction, approximately half of the thickness of the sand above the cushion is replaced and recompacted naturally after each rockfall impact to minimize the impact on the next impact results. Yan et al. [20] mentioned that to ensure the accuracy of the experimental results and eliminate the influence of experimental errors, the experiments under each working condition were carried out at least three times, and the average value of multiple experiments was taken as the experimental result.

3. Experimental Results

The impact force results of five kinds of falling stones under five falling heights were analysed.

The acceleration curves of different shaped drop hammers collected by the dynamic signal acquisition instrument were compared and analysed, as shown in Figure 3. Taking the curve with a drop height of 1.2 m as an example, it can be seen that the acceleration at the initial position of the curve was zero. This was because, at this time, the drop hammer was in a free fall state after the power was cut off by the electromagnet. The acceleration of the drop hammer remained unchanged before contacting the cushion, which was always equal to the gravity acceleration. The acceleration sensor used in this experiment could not collect the constant acceleration but only the variation in the acceleration. Regardless of the shape of the rockfall, the form of the hammer acceleration curve was consistent. After contacting the cushion, the hammer reached the peak acceleration in a very short time except for the D1 hammer, and then the acceleration decreased to zero. D4 and D5 almost reached the peak acceleration at the same time, and the time for D4 and D5 to reach the peak acceleration was earlier than that for D3, D2, and D1. Compared with other shapes of falling stones, D5 and D4 had a large contact area with the cushion. It was observed in the experiment that D5 and D4 moved in the cushion with a short distance; therefore, they could reach the peak acceleration quickly. It can be seen that the duration of the impact also had the following order: D5 > D4 > D3 > D2 > D1. The test results showed that the rockfall shape had an impact on the order of acceleration reaching the peak and the duration of impact, and the impact of rockfall shape could not be ignored when considering the impact time of rockfall.

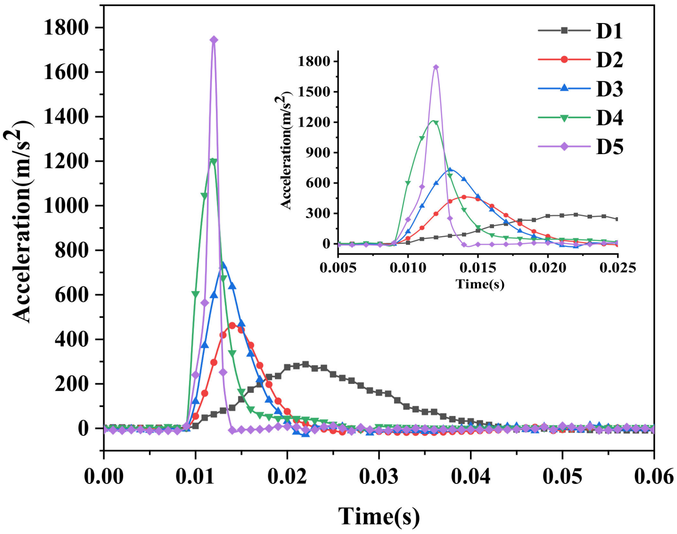

Figure 3. Acceleration time history curves of drop hammers with different shapes impacting the sand cushion.

The impact force results of five shapes of rockfall impacting the sand cushion are shown in Figure 4. The figure shows that the impact force increased with falling height. Under the same falling height, the impact force results always had the law of D1 < D2 < D3 < D4 < D5. The impact force results of D5 were greater than those of sphere D3 commonly used in the impact force model and were much greater than the impact force results corresponding to D1. When the falling height was 1.2 m, the impact force corresponding to D5 was 2.926 kN, the impact force corresponding to D3 was 1.243 kN, and the impact force corresponding to D1 was 0.468 kN. D5 reached six times D1, which fully shows that it is very dangerous to ignore the rockfall shape when considering the rockfall impact problem. When the five falling rocks with the same mass fell at the same falling height, the corresponding initial kinetic energy was the same. Observing the deformation of the cushion behind the impact cushion of the five falling rocks, it can be found that the depression depth corresponding to D5 was much smaller than that corresponding to D1. Combined with the time history curve in Figure 3, taking D5 and D1 as examples, D5 reached the peak acceleration in a very short time, and the impact duration was short with a large impact force. The peak acceleration time of D1 was relatively backwards, and the impact duration was long. The results of the impact force and impact time in the experiment could well match the functional principle.

It can also be seen from Figure 4 that the impact force of rockfall varied nonlinearly with the change in falling height but varied exponentially with a number less than 1. The impact force curve of various shapes of rockfall impacting the sand cushion was fitted in the form of a power function and the impact force $P = \alpha * H$ (falling height) $\hat{}\ ^{\beta}$. The parameters of the fitting formula are shown in Table 3. The exponent of the power function was approximately 0.598, indicating that the change in the rockfall impact force with the falling height was independent of the influence of the rockfall shape on the impact force. The influence of the falling height on the impact force was independent of the rockfall shape. This result is consistent with the commonly used formula for calculating the rockfall impact force in Labiouse et al. [11] and Kawahara et al. [25], in which the impact force is proportional to the 3/5 power of the falling height, indicating that the experimental error is within an acceptable range and the experimental results are reliable. Due to the independence of the falling height, it can be considered that although only five kinds of falling heights were set in this paper to explore the impact of falling stone shapes on the impact force, it was sufficient to explain the situation of multiple falling heights.

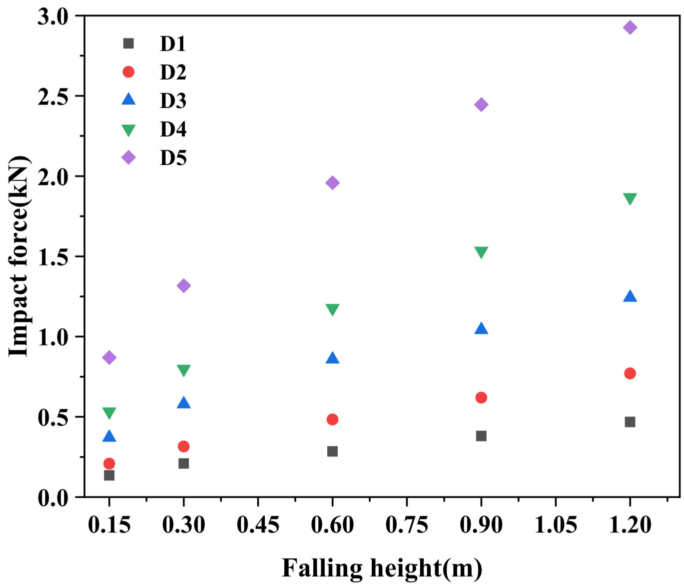

Figure 4. Impact force results of drop hammers with different shapes impacting the sand cushion.

Table 3. First fitting parameters.

No.	α	β
D1	0.41	0.60
D2	0.68	0.64
D3	1.12	0.56
D4	1.65	0.61
D5	2.62	0.58

Based on the current reliable experimental results, the impact force calculation of different shapes of rockfall impacting sand cushions is considered. Since there are many reasonable formulas for calculating the impact force of spherical rockfall, this paper takes the impact force results of spherical D3 as the benchmark and intends to use the shape coefficient S to modify the formula for calculating the impact force. The formula for calculating the impact force P of rockfall is expressed as follows:

$$P = S^k P_{\text{sp}} \tag{1}$$

where P is the rockfall impact force (kN), S is a coefficient describing the shape of rockfall, k is a constant coefficient obtained by fitting, and P_{sp} is the impact force (kN) of spherical rockfall obtained under the same mass and same working conditions.

Considering the five falling heights shown in Figure 4, the average value of the impact force ratio of each rockfall shape to spherical rockfall was taken and fitted. The fitting results are shown in Figure 5.

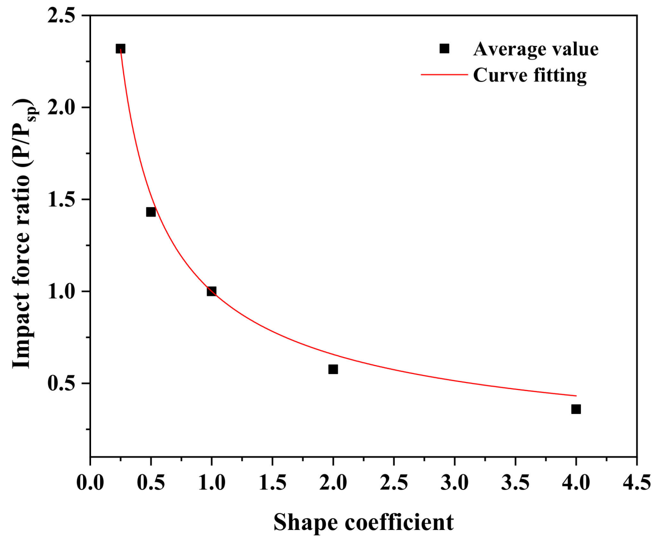

Figure 5. Second fitting results.

By fitting k to approximately -0.6055, the k value was substituted into Equation (1), and the following formula was obtained:

$$P = S^{-0.6055} P_{sp} \tag{2}$$

Equation (2) was used to calculate the impact force of impact sand cushions with different shapes of falling stones at different falling heights, and the results were compared with the experimental results. The impact force corresponding to D3 in Figure 4 is taken from P_{sp}, and the results are shown in Figure 6.

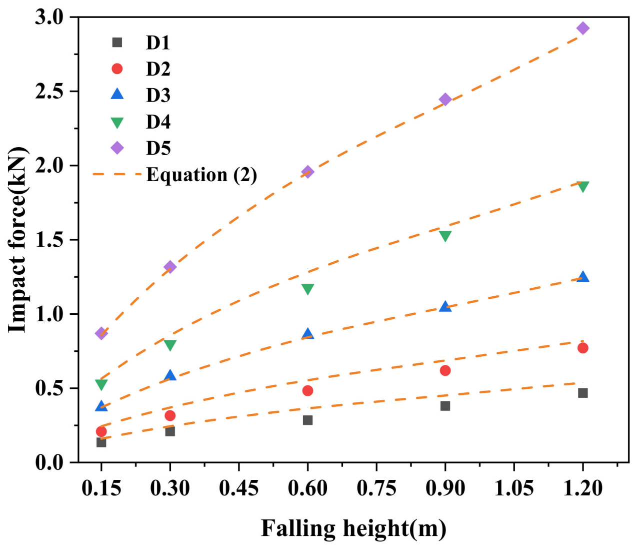

Figure 6. Comparison between fitting results and test results.

From the fitting results in Figure 6, except for individual results, the difference between the two results was less than 20%. In particular, for the D5 rockfall, that is, the maximum impact force and the most unsafe situation, the fitting effect was better, and the difference was only approximately 2%. It can be considered that the impact force calculation formula considering the rockfall shape obtained by Equation (2) has a certain rationality and correctness.

To further verify the rationality of the above fitting formula, the fitting results of the formula were compared with those from other large-scale experiments or numerical simulations. The results are shown in Table 4.

Table 4. Comparison of impact force results of rockfall with different shape coefficients.

S > 1	1.15	1.41	1.71	2.16
Yan [14] Equation (2)	0.93 0.92	0.88 0.81	0.76 0.72	0.51 0.63
S < 1	0.4	0.6		
Wang [18] Equation (2)	1.2~2.0 1.74	1.0~1.5 1.36		

Yan et al. [17] used a numerical method to study the difference in the impact effect between four kinds of tip ellipsoids and spheres. The weight of rockfall was 1358 kg, and the impact velocities were 15.66 m/s, 26.22 m/s, and 36.94 m/s. The impact object was a reinforced concrete slab. Considering the three landing heights, the ratios of the impact force results of the four tip ellipsoids to the sphere were averaged, which were approximately 0.93, 0.88, 0.76, and 0.51. Combined with the concept of the shape coefficient mentioned in this paper, the shape coefficients corresponding to the four tip ellipsoids were 1.15, 1.41, 1.71, and 2.16, respectively. The ratios obtained by Equation (2) were 0.92, 0.81, 0.72, and 0.63, respectively, which are in good agreement with the ratios obtained by Yan et al. through numerical simulation.

Wang [27] utilized three shapes (sphere, cube, and cuboid) and five masses (3.56 kg, 8.88 kg, 11.57 kg, 16.65 kg, and 21.84 kg) of rockfall specimens for rockfall impact shed tunnel model experiments. The cushion layer was a sand cushion, and the thicknesses of the cushion layers were 10 cm, 15 cm, and 20 cm. The experimental results showed that the ratio of the impact force of the cube to the sphere was mostly between 1.2 and 2.0 and that of the cuboid to the sphere was mostly between 1.0 and 1.5. Combined with our fitting formula, the contact area of the square and cuboid rockfall used by Wang was larger than that of the spherical rockfall, which was closer to the situation where the shape coefficient mentioned in this paper was greater than 1. According to Wang's description of the size of the square and cuboid, the shape coefficients were approximately 0.4 and 0.6, respectively. Combined with Equation (2), the ratio of the impact force of the square, cuboid, and spherical rockfall calculated by the method in this paper was approximately 1.74 and 1.36, respectively, which was approximately the middle position of the experimental results obtained by Wang, indicating the reliability of the fitting formula in this paper.

Compared with the results of the above two articles, the rationality of calculating the rockfall impact force of other shapes based on the spherical rockfall impact force is verified. At the same time, it also provides a strong guarantee for the accuracy of the fitting formula in this paper at the corresponding scale.

4. Numerical Model and Discussion

As a common means of scientific research, numerical simulation can intuitively reflect the objective law under the premise of accurate model establishment, which is often used for rockfall impact simulation [28–30]. Due to the limitations of the laboratory experimental site and other factors, the laboratory experimental scale designed in this paper is small, which is quite different from the actual engineering scale. To more comprehensively explore the applicability of the impact force calculation formula introduced into the rockfall shape at a larger engineering scale, the numerical simulation method is used.

4.1. Model Establishment

This paper utilizes the commercial finite element software ANSYS to simulate the process of rockfall impacting shed tunnel cushions. First, a numerical model corresponding to laboratory experiments is established, as shown in Figure 7. The solid element is used in the cushion and rockfall, and the SOLID185 element is selected. The contact between the rockfall and cushion is surface–surface contact. The lower surface of the rockfall is the target surface, and the TARGE170 element is selected. The upper surface of the cushion is the contact surface, and the CONTA174 element is selected. The size of the cushion is 1 m × 1 m × 0.3 m. Using the bilinear constitutive model, the elastic parameters of the material are consistent with the material parameters of the sand cushion used in the experiment, as shown in Table 5. The selection of the yield stress and tangent modulus is based on the calculation method and reference range mentioned by Wang et al. [31]. The constitutive model curve is shown in Figure 8.

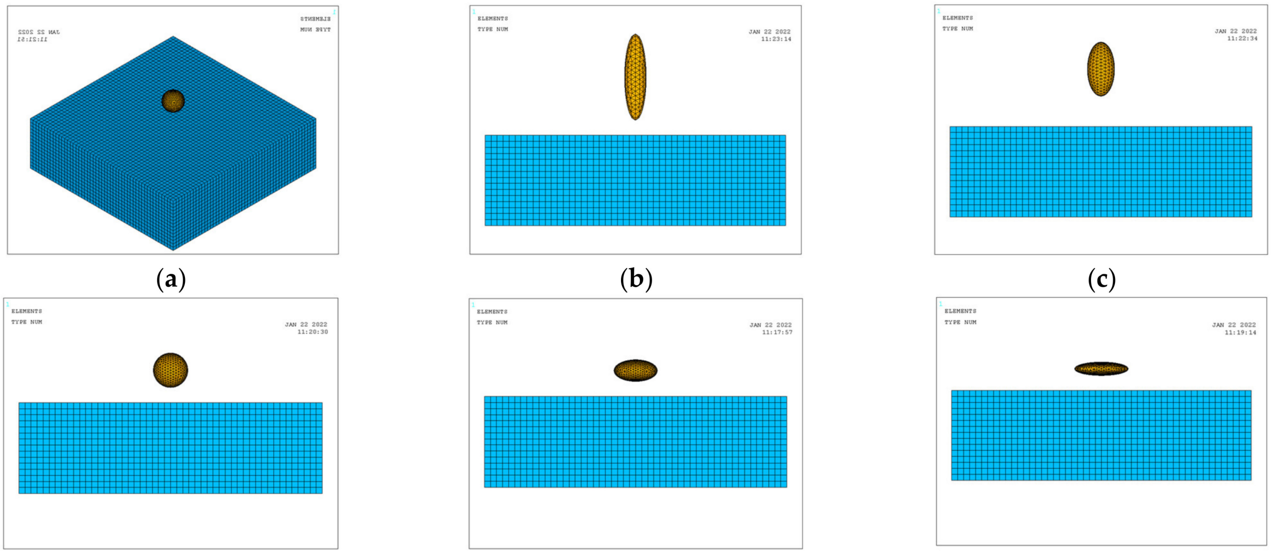
(a) (b) (c) (d) (e) (f)

Figure 7. Numerical model. (**a**) The numerical model used in this article as a three-dimensional model. (**b**) D1 rockfall impact sand cushion, (**c**) D2 rockfall impact sand cushion. (**d**) D3 rockfall impact sand cushion, (**e**) D4 rockfall impact sand cushion, and (**f**) D5 rockfall impact sand cushion.

Table 5. Mechanical parameters of each material.

Material	Density (kg/m^3)	Elastic Modulus (MPa)	Poisson Ratio
Rock block	2135	25,000	0.20
Sand cushion	1600	39	0.20

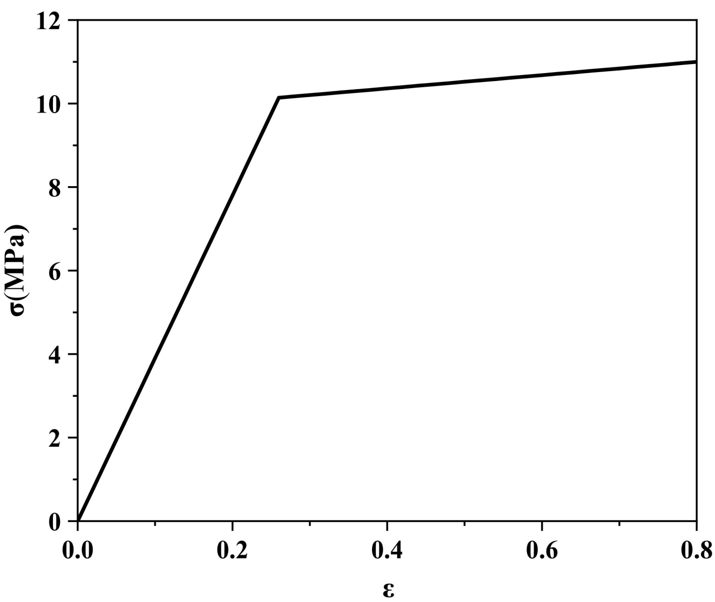

Figure 8. Constitutive model curve of the cushion material.

All freedoms at the bottom of the cushion are constrained. Rockfall material is simplified as an elastic material with large stiffness. The mass of the rockfall is 1.65 kg, and the shape of the rockfall is ellipsoid with different ratios of long axis to short axis. The size is consistent with the laboratory experiment. The size is shown in the following Table 2. The radius of the ellipsoid in the falling direction is b, and the radius in the vertical direction is $c = d/2$.

4.2. Model Correction

The falling rocks of five shapes are dropped at heights of 0.15 m, 0.3 m, 0.6 m, 0.9 m, and 1.2 m to obtain the acceleration curves of falling rocks of different shapes at different heights. The product of the maximum acceleration and the mass of falling rocks is taken as the impact force of falling rocks of different shapes at different heights. The impact force results obtained by numerical simulation are compared with those obtained by laboratory experiments, and the comparison results are shown in Figure 9.

It can be seen from Figure 9 that, in general, regardless of the shape and height of falling rocks, the two results are relatively close, showing a trend that the numerical simulation results are larger than the experimental results in the laboratory. The reason for the large numerical simulation results is mainly that, compared with the real laboratory experiments, the numerical model is an ideal model, and the kinetic energy of falling rock may be dissipated by friction heat generation or in other ways that are not considered. The red number in Figure 9 represents the absolute value of the difference between the two results. Except for individual points, the difference between the two results is controlled within 20%, and the two impact forces of the flat ellipsoid with a large and relatively dangerous impact force are very close. Especially when the landing height is 1.2 m, the difference between the two results is only 0.43%. Therefore, it can be considered that the establishment of a numerical model and the selection of model parameters are more accurate, and the numerical results are more reliable, which can basically reflect the real situation of the impact force.

4.3. Large-Scale Model

The accuracy of the numerical model is corrected by comparing the numerical simulation results at the laboratory scale with the experimental results. Considering the actual engineering scale, the rockfall impact energy level is much greater than the impact energy level corresponding to laboratory experiments. Therefore, based on this model, considering a larger and closer rockfall impact model to the actual engineering scale, the rockfall impact process with an impact energy level of 180 kJ is simulated. It is worth noting that an energy level of 180 kJ has a variety of conditions. This paper only selected three conditions. With rock block and cushion material parameters unchanged, the falling rock shape is still set to five kinds. The falling stone masses are 1000 kg, 1500 kg, and 2000 kg. The falling height corresponds to 18 m, 12 m, and 9 m. The cushion size is 5 m $\times$ 5 m, and the cushion thickness is set to1.5 m, which is commonly used in engineering. The specific size of falling stone is shown in Table 6.

When the energy level is fixed to 180 kJ, the impact force results of falling rocks with five shapes of different masses at corresponding heights are shown in Figure 10. The results are compared with those calculated by using the impact force results of spherical rockfall in numerical simulation as the benchmark and combining with the modified formula proposed in this paper.

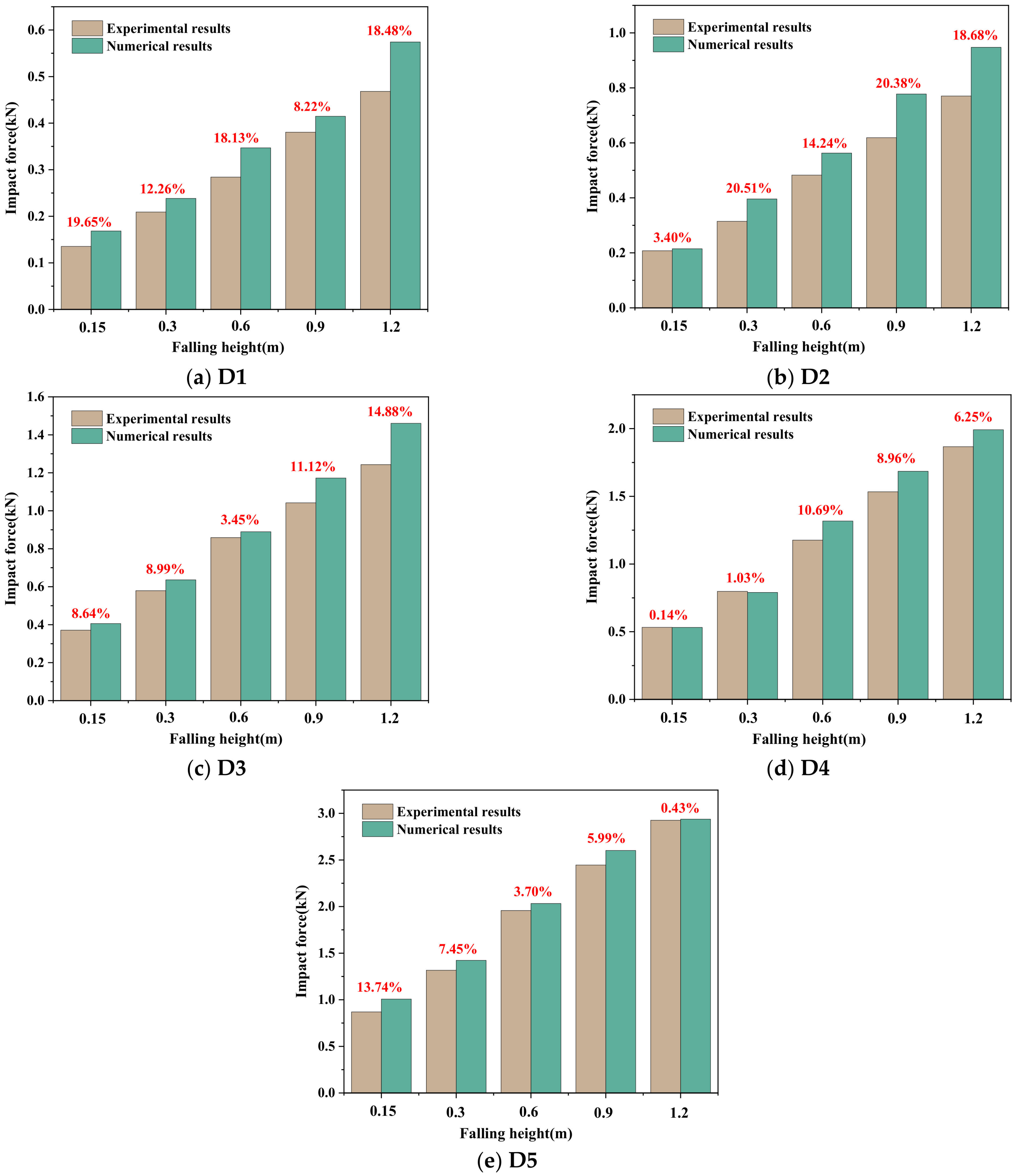

Figure 9. Comparison of the experimental results and numerical results of five shapes of falling rocks at five falling heights. (**a**–**e**) correspond to five different shapes of rockfall, respectively.

Table 6. Large size simulation of falling rock size.

Case	Falling Height(m)	Shape Coefficient	Mass (kg)	Vertical Radius (m)	Horizontal Radius (m)
Case 1	18	4	992.582	1.12	0.28
		2	1011.456	0.71	0.355
		1	1002.852	0.446	0.446
		0.5	992.582	0.28	0.56
		0.25	1011.456	0.1775	0.71
Case 2	12	4	1481.638	1.28	0.32
		2	1501.852	0.81	0.405
		1	1499.487	0.51	0.51
		0.5	1481.638	0.32	0.64
		0.25	1501.852	0.2025	0.81
Case 3	9	4	2022.913	1.42	0.355
		2	2060.154	0.9	0.45
		1	1985.163	0.56	0.56
		0.5	2022.913	0.355	0.71
		0.25	2060.154	0.225	0.9

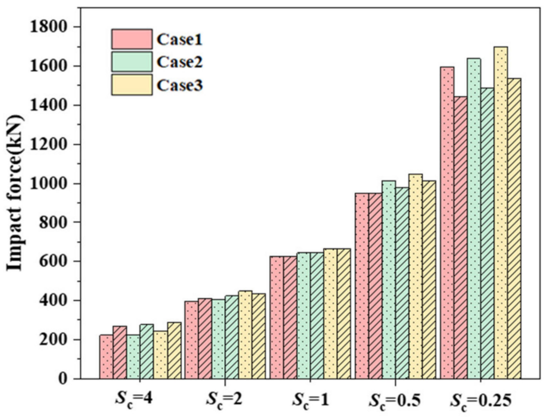

Figure 10. Comparison of large-scale simulation results and fitting results under three conditions. Speckles represent the results of numerical simulation, and diagonals represent the results obtained by Equation (2).

It can be seen from the numerical simulation results of Case 1, Case 2, and Case 3 in Figure 10 that the shape of rockfall does affect the impact force of rockfall. Rockfall impact force decreases with the increase in shape coefficient *S*. When the impact energy level increases, the effect of rockfall shape on rockfall impact force is also obvious. When the impact energy is the same, the impact force corresponding to different mass and height combinations is approximately equal. However, the impact force corresponding to the condition of large mass and small height is slightly larger than that of small mass and large height. That is, the impact force of the three conditions is: Case 1 < Case < Case 3.

As shown in Figure 10, the numerical results are compared with the results of the formula in this paper. Consider the three cases of Case1, Case2, and Case3. For the tip ellipsoid with a shape factor greater than 1, the difference between the two results is slightly larger, and the maximum difference is about 18.7%. When the shape coefficient *S* is less than 1, the two results are close. Especially when $S = 0.5$ in Case 2, the difference is only 0.2%. Therefore, it can be considered that the impact force fitting formula considering rockfall shape proposed in this paper is not only limited to the small-scale model but also applicable to the case of scale increase, which can provide guidance for engineering practices.

4.4. Discussion

In this section, the application scope of the correction formula is expanded by numerical simulation of the large-scale rockfall impact process. However, the formula proposed in this paper also has certain limitations. First of all, this paper only considers the frontal collision between the rockfall and the cushion, that is, assuming the rockfall is free-falling, without considering the horizontal component of the impact force. The behaviour pattern of rockfall is various [32], and the oblique collision behaviour between rockfall and shed tunnel cushion occurs occasionally [33]. Secondly, this paper only assumes that the shed tunnel cushion is a single sand cushion. Many studies have shown that when using some lightweight and high strength cushioning materials instead of sand, the cushioning efficiency of the composite cushion is better. Finally, the correction formula in this paper is obtained by fitting the test results. Although it can well reflect the actual situation, it is still necessary to obtain a more objective impact force algorithm through theoretical derivation.

In addition, this paper focuses on the impact of different shapes of rockfall on shed tunnel cushions. However, in the design of the shed tunnel structure, the penetration depth of the cushion and the diffusion mechanism of impact force in cushion soil is also very important. Therefore, the influence of rockfall shape on penetration depth and diffusion mechanism is also worth exploring. The penetration depth of the cushion cannot be accurately measured due to various reasons, but this problem can be avoided in numerical simulation. Taking the results of numerical simulation when the falling height is 0.9 m as an example, this paper briefly expounds on the influence of falling stone shape on penetration depth and diffusion mechanism.

4.4.1. Penetration Depth

The maximum penetration depth of rockfall with different shapes impacting sand cushion at the same height is shown in Figure 11.

It can be found from the penetration depth shown in Figure 11 that the maximum penetration depth corresponding to different shapes of falling stones and the area with obvious deformation on the top of the cushion are different. The maximum penetration depth increases with the increase in shape coefficient. The maximum penetration depth of the falling rock with $S = 4$ is 68.237 mm. The maximum penetration depths of the falling rock with $S = 2$, 1, 0.5, and 0.25 are 30.033 mm, 21.729 mm, 13.696 mm, and 4.240 mm, respectively. The maximum penetration depth of rockfall with different shapes is very different. The maximum penetration depth of rockfall with $S = 4$ is about 16 times of that with $S = 0.25$. Therefore, even if the rockfall impact force with large shape coefficient is small, the influence of rockfall on impact response cannot be ignored in the structural design of the shed tunnel. The area of deformation caused by $S = 0.25$ rockfall on the top surface of the cushion is significantly larger than that caused by $S = 4$. This is mainly related to the area at the bottom of the rockfall. The lower surface curvature radius of the rockfall with $S = 0.25$ is larger, and the contact surface with the cushion is larger. The lower surface curvature radius of the rockfall with $S = 4$ is smaller, and the contact surface with the cushion is smaller. When the penetration depth of cushion is the same, the larger the contact area (the smaller the shape coefficient) is and the more the kinetic energy of rockfall is consumed. Therefore, when the initial kinetic energy of rockfall is constant compared with larger shape coefficient and spherical rockfall, the rockfall with a smaller shape coefficient needs greater penetration depth to consume the kinetic energy of rockfall. The maximum penetration depth increases with the increase in the shape coefficient.

Furthermore, the phenomenon of different impact forces corresponding to different shapes of rockfall can be explained by the different maximum penetration depths corresponding to different shapes of rockfall. When rockfalls with different shapes fall at the same height, the tip rockfall is easier to move downward in the cushion than the flat rockfall, and the contact time with the cushion is longer. The corresponding penetration depth is larger, and the impact process is slower, so the corresponding impact force is smaller.

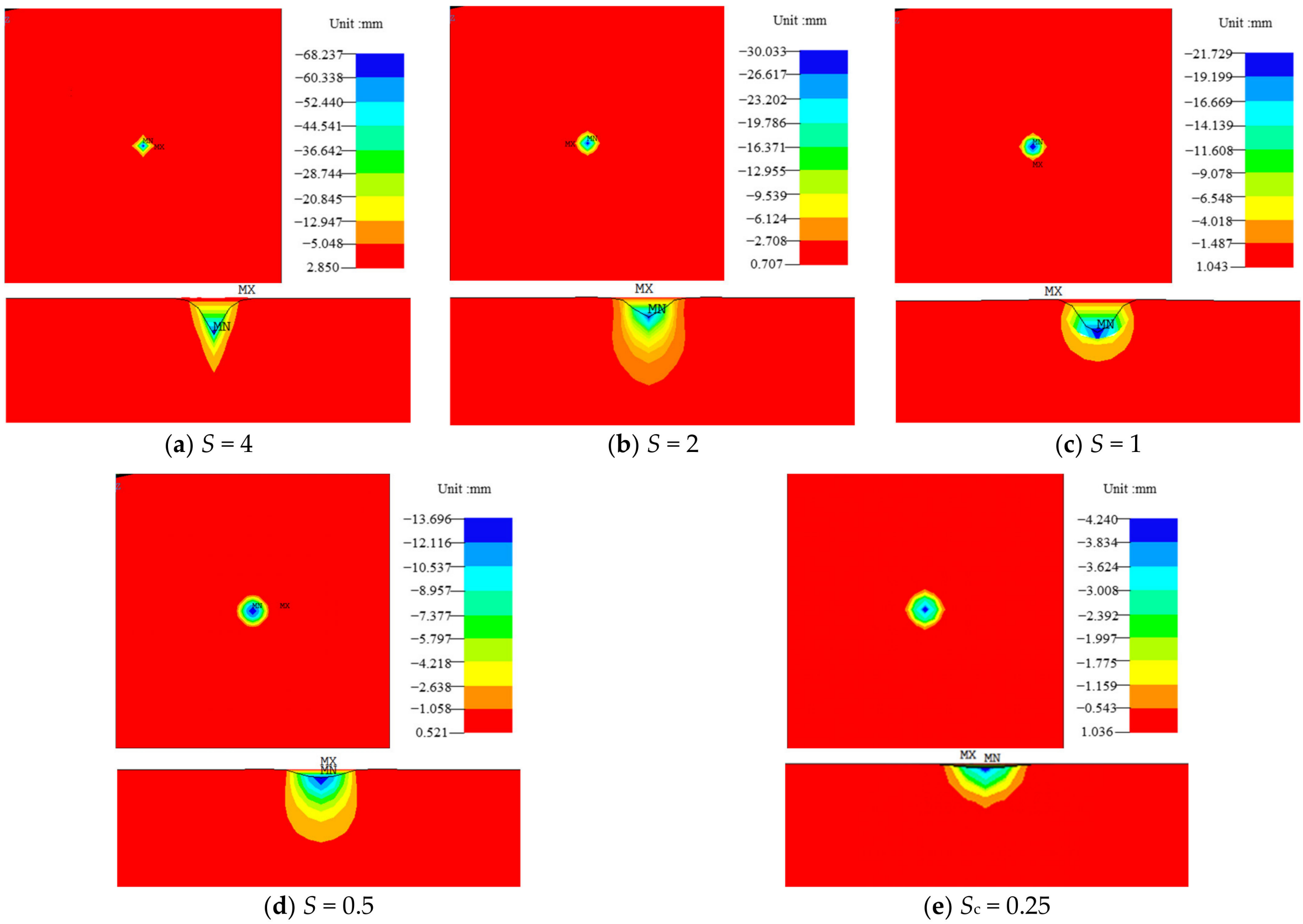

Figure 11. Penetration depth of sand cushion impacted by falling stones of different shapes in numerical simulation. (**a**–**e**) correspond to five different shapes of rockfall, respectively.

4.4.2. Diffusion Mechanism

As shown in Figure 11, when rockfalls with different shapes impact the cushion, the impact force is different, and the area of deformation on the top surface of the cushion is affected by the impact is different. Therefore, it is necessary to study the diffusion of impact stress caused by different shapes of rockfall in the cushion. Figure 12 shows the magnitude of vertical stress in the cushion corresponding to falling stones with shape coefficients of 0.5 and 2, respectively.

It can be seen from Figure 12 that the impact stress diffusion mechanisms correspond to falling rocks with a shape coefficient less than 1 and greater than 1. The impact of falling rock corresponding to the large shape coefficient is small, the contact area with the cushion is small, and the diffusion range of impact stress in the cushion is small. However, the cushion will lead to greater impact stress. Therefore, the influence of rockfall shape cannot be ignored when considering the impact of stress diffusion in the cushion. The tip ellipsoid experiences greater impact stress.

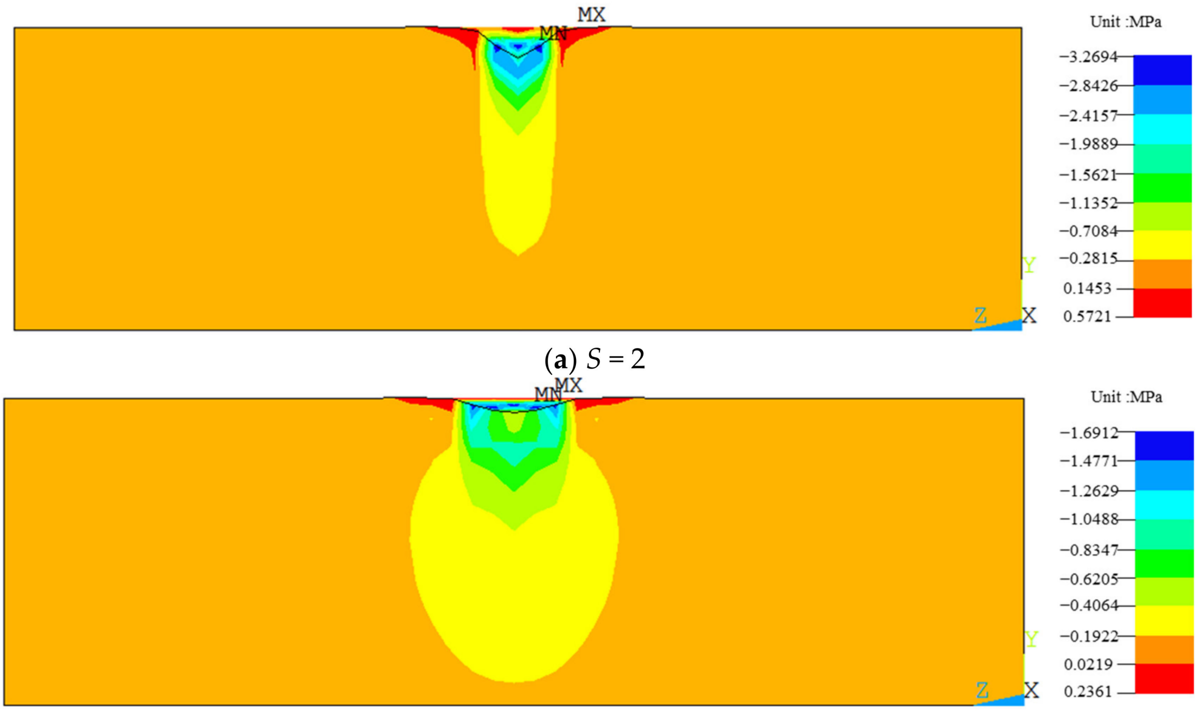

(**a**) $S = 2$

(**b**) $S = 0.5$

Figure 12. Impact stress in the sand cushion corresponding to falling stones of different shapes in numerical simulation. (**a**) and (**b**) represent rockfall with shape coefficients of 2 and 0.5, respectively.

5. Conclusions

Based on laboratory experiments, this paper explores the influence of rockfall shape on rockfall impact force. By fitting the experimental data, a formula of rockfall impact force considering rockfall shape is given, which is verified by comparison with the research results from other studies, and the reliability of the numerical model is corrected. The applicability of the fitting formula is further promoted by establishing a large-scale numerical model, and some considerations are triggered. The conclusions are as follows:

(1) The influence of rockfall shape on rockfall impact force cannot be ignored. It is unsafe to ignore the influence of the rockfall shape in the calculation formula of the rockfall impact force. On the basis of the spherical rockfall impact force, a coefficient considering rockfall shape is added to correct the calculation formula of the rockfall impact force.

(2) The influence of the falling height on the impact force of rockfall is independent and is not affected by the rockfall shape. The impact force changes with the falling height with a power function with less than 1 as the index.

(3) At the same energy level, the impact force of different working conditions is roughly the same. However, there is still the fact that the impact force corresponding to large mass is greater than small mass. The condition of large mass and small height is relatively more dangerous.

(4) The shed-tunnel structure usually sets a buffer cushion above the concrete slab to disperse and absorb the impact energy. The impact force is dispersed through the cushion and transmitted to the plate and frame. Therefore, accurately obtaining the rockfall impact force acting on the cushion of the shed tunnel can provide a basis for the selection of the most unfavourable load in the design of the shed tunnel structure.

(5) In the design of the shed-tunnel structure, in addition to the physical quantity of rockfall impact force, the penetration depth and the diffusion mechanism of impact force in the cushion cannot be ignored.

In this paper, the correction of the rockfall impact force is obtained by fitting the laboratory experimental data. The impact force calculation formula considering the rockfall shape can be carried out based on theory. At present, it is only assumed that the cushion is a single cushion, and the composite cushion is not considered.

Author Contributions: Conceptualization, Y.Z. and P.Z.; methodology, Y.Z. and B.H.; software, Y.Z. and P.Z.; validation, L.X., B.H. and P.Z.; formal analysis, Y.Z.; investigation, Y.Z.; resources, L.X.; data curation, Y.Z.; writing—original draft preparation, Y.Z.; writing—review and editing, L.X., B.H. and P.Z.; visualization, Y.Z.; supervision, L.X. and B.H.; project administration, B.H. All authors have read and agreed to the published version of the manuscript.

Funding: This research was funded by Department of Transportation of Sichuan Province, grant number 2020-MS3-101/2020-B-01.

Institutional Review Board Statement: Not applicable.

Informed Consent Statement: Not applicable.

Data Availability Statement: This study did not report any data.

Acknowledgments: We thank AJE (www.aje.cn accessed on 17 February 2022) for its linguistic assistance during the preparation of this manuscript.

Conflicts of Interest: The authors declare no conflict of interest.

References

1. Abdelmaboud, A.; Abaker, M.; Osman, M.; Alghobiri, M.; Abdelmotlab, A.; Dafaalla, H. Hybrid Early Warning System for Rock-Fall Risks Reduction. *Appl. Sci.* **2021**, *11*, 9506. [CrossRef]
2. Bao, F.; Hu, R. Application of the Shed Hole on the Yu-Xiang express way. *Highway* **2009**, *10*, 260–262.
3. Wang, Q.; Wang, L.; Li, Z.; Wang, H.; Xu, X. Open tunnel engineering and secondary disasters of earthquake in the post-earthquake reconstruction projects along Duwen road. *J. Mt. Sci.* **2011**, *29*, 356–361.
4. Zhao, P.; Xie, L.; Li, L.; Liu, Q.; Yuan, S. Large-scale rockfall impact experiments on a RC rock-shed with a newly proposed cushion layer composed of sand and EPE. *Eng. Struct.* **2018**, *175*, 386–398. [CrossRef]
5. He, S.; Shen, J.; Wu, Y. Rock shed dynamic response to impact of rock-fall. *Rock Soil Mech.* **2011**, *32*, 781–788.
6. Yang, L.; Li, S.; Wu, Z.; Shen, X. Dynamic analysis of rock-fall impact on shed tunnel structure. *J. Traffic Transp. Eng.* **2012**, *12*, 25–30.
7. Wang, L.; Liu, L.; Tang, F.; Tang, H. Study on Impact Force of Rockfall Impact Experiment on Shed Tuunel. *J. Disaster Prev. Mitig. Eng.* **2018**, *38*, 973–979.
8. Zhao, P.; Xie, L.; He, B.; Zhang, Y. Experimental study of rock-sheds constructed with PE fibres and composite cushion against rockfall impacts. *Eng. Struct.* **2018**, *177*, 175–189. [CrossRef]
9. Calvetti, F.; Di Prisco, C. Rockfall impacts on sheltering tunnels: Real-scale experiments. *Géotechnique* **2012**, *62*, 865–876. [CrossRef]
10. Breugnot, A.; Lambert, S.; Villard, P.; Gotteland, P. A Discrete/continuous Coupled Approach for Modeling Impacts on Cellular Geostructures. *Rock Mech. Rock Eng.* **2015**, *49*, 1831–1848. [CrossRef]
11. Labiouse, V.; Descoeudres, F.; Montani, S. Experimental Study of Rock Sheds Impacted by Rock Blocks. *Struct. Eng. Intern.* **1996**, *6*, 171–176. [CrossRef]
12. Ferrari, F.; Giacomini, A.; Thoeni, K. Qualitative Rockfall Hazard Assessment: A Comprehensive Review of Current Practices. *Rock Mech. Rock Eng.* **2016**, *49*, 2865–2922. [CrossRef]
13. Di Luzio, E.; Mazzanti, P.; Brunetti, A.; Baleani, M. Assessment of tectonic-controlled rock fall processes threatening the ancient Appia route at the Aurunci Mountain pass (central Italy). *Nat. Hazards* **2020**, *102*, 909–937. [CrossRef]
14. Wang, B.; Cavers, D.S. A simplified approach for rockfall ground penetration and impact stress calculations. *Landslides* **2008**, *5*, 305–310. [CrossRef]
15. Perera, S.; Lam, N.; Pathirana, M.; Zhang, L.; Ruan, D.; Gad, E. Deterministic solutions for contact force generated by impact of windborne debris. *Intern. J. Impact Eng.* **2016**, *91*, 126–141. [CrossRef]
16. Chen, C.; Liu, C.; Chen, L.; Zhao, S. Study on Impact Force of Rock-fall onto Rock Shed Tunnel. *J. Highw. Transp. Res. Dev.* **2015**, *32*, 102–109.
17. Yan, P.; Zhang, J.; Fang, Q.; Zhang, Y. Numerical simulation of the effects of falling rock's shape and impact pose on impact force and response of RC slabs. *Constr. Build. Mater.* **2018**, *160*, 497–504. [CrossRef]
18. Shen, W.; Zhao, T.; Dai, F.; Jiang, M.; Zhou, G.G.D. DEM analyses of rock block shape effect on the response of rockfall impact against a soil buffering layer. *Eng. Geol.* **2019**, *249*, 60–70. [CrossRef]
19. Ji, Z.; Chen, Z.; Niu, Q.; Wang, T.; Song, H.; Wang, T. Laboratory study on the influencing factors and their control for the coefficient of restitution during rockfall impacts. *Landslides* **2019**, *16*, 1939–1963. [CrossRef]

20. Yan, P.; Fang, Q.; Zhang, J.; Zhang, Y.; Chen, L.; Fan, J. Experimental study and dimensionless analysis of rockfall impacts on the sand cushion considering different typical shapes of falling rocks. *Explos. Shock Waves* **2021**, *41*, 96–111.
21. Yu, Z.; Luo, L.; Liu, C.; Guo, L.; Qi, X.; Zhao, L. Dynamic response of flexible rockfall barriers with different block shapes. *Landslides* **2021**, *18*, 2621–2637. [CrossRef]
22. Yu, B.; Yi, W.; Zhao, H. Experimental study on the maximum impact force by rock fall. *Landslides* **2017**, *15*, 233–242. [CrossRef]
23. Ministry of Transport of the People's Republic of China. 1995. Available online: https://www.mot.gov.cn/shuju/ (accessed on 17 February 2022).
24. Yang, Q.; Guan, B. Test and research on calculating method of falling stone impulsive force. *J. China Railw. Soc.* **1996**, *18*, 101–106.
25. Kawahara, S.; Muro, T. Effects of dry density and thickness of sandy soil on impact response due to rockfall. *J. TerraMech.* **2006**, *43*, 329–340. [CrossRef]
26. Seguin, A.; Bertho, Y.; Martinez, F.; Crassous, J.; Gondret, P. Experimental velocity fields and forces for a cylinder penetrating into a granular medium. *Phys. Rev. E Stat. Nonlin. Soft Matter Phys.* **2013**, *87*, 012201. [CrossRef]
27. Guangkun, W. *Research on Shed Structure for Rockfall Impact*; Chongqing Jiaotong: Chongqing, China, 2014.
28. Plassiard, J.P.; Donzé, F.V. Rockfall impact parameters on embankments: A discrete element method analysis. *Struct. Eng. Intern. J. Intern. Assoc. Bridge Struct. Eng.* **2009**, *19*, 333–341. [CrossRef]
29. Dong, F.; Bie, X.; Tian, J.; Xie, X.; Du, G. Experimental and Numerical Study on the Strain Behavior of Buried Pipelines Subjected to an Impact Load. *Appl. Sci.* **2019**, *9*, 3284. [CrossRef]
30. Wang, H.; Guo, C.; Wang, F.; Ni, P.; Sun, W. Peridynamics simulation of structural damage characteristics in rock sheds under rockfall impact. *Comput. Geotech.* **2022**, *143*, 104625. [CrossRef]
31. Wang, Y.; Xu, M.; Yang, C.; Lu, M.; Meng, J.; Wang, Z.; Wang, M. Effects of elastoplastic strengthening of gravel soil on rockfall impact force and penetration depth. *Intern. J. Impact Eng.* **2020**, *136*, 103411. [CrossRef]
32. Liao, X.; Ouyang, Q.; Liu, H.; Sun, J.; Wang, X.; Li, L.; Yang, Z.; Chen, Z. Experimental Study on Rockfall Mechanism of Platy Rock on a Complex Slope. *Appl. Sci.* **2020**, *10*, 2849. [CrossRef]
33. Azarafza, M.; Akgun, H.; Feizi-Derakhshi, M.R.; Azarafza, M.; Rahnamarad, J.; Derakhshani, R. Discontinuous rock slope stability analysis under blocky structural sliding by fuzzy key-block analysis method. *Heliyon* **2020**, *6*, e03907. [CrossRef]